Rab7 regulates maturation of melanosomal matrix protein gp100/Pmel17/Silv

Akinori Kawakami, Fumio Sakane*, Shin-ichi Imai*, Satoshi Yasuda*, Masahiro Kai*, Hideo Kanoh*, Hai-Ying Jin, Kuninori Hirosaki, Toshiharu Yamashita, and Kowichi Jimbow†
Departments of Dermatology and *Biochemistry (Section II), Sapporo Medical University School of Medicine, Sapporo, Japan

† Corresponding author: Kowichi Jimbow, MD、PhD, FRCPC
From the Department of Dermatology, Sapporo Medical University School of Medicine, South-1, West-16, Chuo-ku, Sapporo, 060-8543, Japan. Tel: +81-11-611-2111 ext. 3460, Fax: +81-11-613-3739, E-mail: jimbow@sapmed.ac.jp

Short title
Rab7 regulates gp100 maturation

Abbreviations
TGN: trans-Golgi network; TYRP-1: tyrosinase-related protein 1; YFP: yellow fluorescent protein; WT: wild type; PBS, phosphate-buffered saline

ABSTRACT
Melanosome biogenesis consists of multi-step processes that involve protein synthesis, vesicle transport/fusion and post-translational modifications such as glycosylation, proteolysis and oligomerization. Because of the complexity, detailed molecular mechanism of melanosome biogenesis is still elusive. Here we found that, in MMAc melanoma cells, wild-type (WT) Rab7 and its dominant active mutant (Rab7-Q67L), but not its dominant negative mutant (Rab7-T22N), were co-localized in the perinuclear region with granules containing Stage I-melanosomes where the full-length, immature gp100/Pmel17/Silv was present. We also found that over-expression of Rab7-Q67L and, to a lesser extent, Rab7-WT increased the amount of proteolytically processed, mature gp100 in MMAc cells. However, Rab7-T22N did not show such effect. Moreover, siRNA-mediated Rab7-knockdown considerably inhibited the gp100 maturation. These results collectively suggest that the GTP-bound form of Rab7 promotes melanogenesis through the regulation of gp100 maturation in melanoma cells.

Keywords: Rab7; gp100; Melanosome; Transport; Processing; Melanogenesis; GTPase

INTRODUCTION
The Rab family small G proteins are known to be key regulators of intracellular vesicle traffic, including exocytosis and endocytosis. In mammalian cells, more than 60 Rab members have been identified and each member localizes at the surface of a distinct intracellular compartment (Pfeffer, 1999; Somsel Rodman and Wandinger-Ness, 2000; Takai et al., 2001; Zerial and McBride, 2001). The Rab GTPases serve as molecular switches that are activated on GTP binding and inactivated following nucleotide hydrolysis, concomitantly cycling between the

cytosol (GDP-bound, inactive form) and the membranes (GTP-bound, active form). To facilitate vesicle traffic, the GTPases regulate one (or several) specific step(s) of vesicle traffic by the recruitment of the tethering/docking and fusion factors and the actin- and microtubule-based motor proteins (Chabrillat et al., 2005; Harrison et al., 2003; Kuroda et al., 2003; Strom et al., 2002; Wu et al., 2001).

Rab7 is present on late endosomes and lysosomes, and controls membrane trafficking between the early and late endosomes (Press et al., 1998), and from the late endosomes to lysosomes (Feng et al., 1995; Meresse et al., 1995; Vitelli et al., 1997). Rab7 has also been implicated in lysosome biogenesis by regulating the heterotypic fusion between late endosomes and lysosomes, and the homotypic fusion of lysosomes (Bucci et al., 2000). Recently, some Rab7 target proteins such as Rab-interacting lysosomal protein (Cantalupo et al., 2001; Harrison et al., 2003), Rab-interacting RING finger protein (Mizuno et al., 2003), hVPS34/p150 (Stein et al., 2003), proteasome □-subunit XAPC7 (Dong et al., 2004), and oxysterol-binding protein homologue ORP1L (Johansson et al., 2005) have been identified and characterized. Moreover, we have recently identified Rab7 as a melanosome-associated protein and proposed that Rab7 is involved in the transport of tyrosinase-related protein 1 (TYRP-1) and tyrosinase from the trans-Golgi network (TGN) to melanosomes (Gomez et al., 2001; Hirosaki et al., 2002).

Melanosome biogenesis consists of four stages of maturation with distinct morphological and biochemical characteristics that reflect subcellular processes of the transport of structural and enzymatic proteins and their subsequent structural organization as well as melanin deposition (Jimbow et al., 2000). gp100/Pmel17/Silv is one of the most enigmatic proteins in melanosome biogenesis. After synthesis, gp100 is transported from the TGN to stage I melanosomes, which contain internal membranous vesicles that resemble late-endosomal multivesicular bodies, and is cleaved into several fragments, which form the fibrillar matrix of the organelle (Theos et al., 2005). In the subsequent stages of maturation, melanosomes under eumelanogenesis always exhibit an ellipsoidal shape and form regular parallel intralumenal fibers (Stage II). Melanins are deposited on these fibers, resulting in a progressively pigmented internal matrix (Stage III). Melanin synthesis and deposition continue until little or no internal structure becomes visible (Stage IV). However, the precise mechanism of melanosome biogenesis is still unclear.

To clarify the molecular mechanism of melanosome biogenesis in more detail, we analyzed the functional relationship between Rab7 and gp100. Interestingly, we found that Rab7 was co-localized with gp100 in Stage I melanosomes. Moreover, our studies revealed that Rab7 may play an important role in promoting the gp100 maturation.

RESULTS

Rab7 is co-localized with full-length gp100 in Stage I melanosomes

To explore the functional relationship between Rab7 and gp100, we first examined, by using a confocal microscope, the subcellular localization of Rab7 and the endogenous, full-length gp100, which is distributed in Stage I melanosomes and recognized by anti-gp100 antibody, □PEP13h (Yasumoto et al., 2004). In addition to the full-length gp100, however, □PEP13h is able to recognize the C-terminal fragments (~27-kDa) of gp100 generated by proteolysis as well (see Figure 3a). In Western blotting using hard gels (12% acrylamide), the signal intensities of the 100-kDa band (full-length gp100) were almost the same or at most only two-fold

higher when compared with those of the 27-kDa band (a cleavage product) (See Figures 4a and 5a). However, when a soft gel (6% acrylamide), in which larger proteins including the full-length gp100 are more effectively transferred to a PVDF membrane, was used, the signal intensities of the 100-kDa band (6% acrylamide gel) became 5.2 ± 0.4-fold higher (mean ± S.E., n = 3) than those of the 27-kDa band (12% acrylamide gel) (data not shown). Thus, we consider that □PEP13h mainly recognized the full-length gp100 in MMAc cells. Moreover, the C-terminal fragments are not likely to be carried over to Stage II and later Stage melanosomes because the fragments are unstable and rapidly degraded before the stage of melanosome shifts from I to II (Yasumoto et al., 2004). Thus, this antibody is considered to detect solely gp100 (mainly full-length gp100 and small amounts of its C-terminal fragments) in Stage I melanosomes in melanoma cells.

In addition, MMAc cells were transiently transfected with either the pEYFP empty vector, pEYFP-Rab7-wild-type (WT), pEYFP-Rab7-Q67L (a GTPase-deficient, dominant active mutant) or pEYFP-Rab7-T22N (a GDP-bound, dominant negative mutant). We found that yellow fluorescent protein (YFP)-Rab7-WT and YFP-Rab7-Q67L were visualized as punctuated structures and considerably co-localized with the endogenous full-length gp100 in the perinuclear region (Figure 1). When endogenous Rab7 was detected using indirect immunofluorescence, essentially the same result was obtained (data not shown). In contrast, YFP-Rab7-T22N exhibited a diffuse intracellular localization pattern and failed to be co-localized with the full-length protein. Similar results were obtained with endogenous MART-1, which was reported to interact and co-localize with gp100 in melanoma cells (De Maziere et al., 2002; Hoashi et al., 2005), thus confirming that this gp100-interacting protein was partly co-localized with YFP-Rab7-WT and YFP-Rab7-Q67L, but not with YFP-Rab7-T22N in MMAc cells (data not shown).

To substantiate the melanosomal distribution of Rab7, we investigated whether Rab7-WT and Rab7-Q67L were co-localized with LAMP-2, which is co-localized with the full-length gp100 stained with □PEP13h in the perinuclear region in melanocytes and SK-MEL-28 melanoma cells (Hoashi et al., 2005). We also confirmed the co-localization between LAMP-2 and □PEP13h-recognized gp100 in the peri-nuclear region in MMAc cells (data not shown). As shown in Figure 2, YFP-Rab7-WT and YFP-Rab7-Q67L, but not YFP-Rab7-T22N, were co-localized exclusively with this marker protein (LAMP-2) in the perinuclear region of MMAc melanoma cells. On the other hand, the cis-Golgi marker GM130 and the endoplasmic reticulum marker KDEL failed to exhibit any co-localizations (data not shown). Taken together, these results suggest that the GTP-bound form of the Rab7 protein is, at least in part, distributed to Stage I melanosomes, with which the full-length gp100 is associated in MMAc melanoma cells.

To validate that the GTP-bound form of Rab7 is associated with Stage I, but not Stage II–IV, melanosomes, MMAc cells were stained with another anti-gp100 antibody HMB45, which recognizes only the processed, mature gp100 (Hoashi et al., 2006) (Figure 3a). Interestingly, neither YFP-Rab7-WT nor YFP-Rab7-Q67L was co-localized with the mature gp100 (Figure 3b), further supporting the localization of Rab7-WT and Rab7-Q67L to Stage I, but not Stage II–IV, melanosomes. These results collectively suggest that the GTP-bound form of Rab7 protein is, at least in part, co-localized with the full-length gp100 in Stage I melanosomes.

Rab7 and its dominant-active mutant (Rab7-Q67L) promote the maturation of

gp100

It is known that the cleavage events of gp100 as a part of its maturation process occur in Stage I melanosomes (Yasumoto et al., 2004). Thus, the finding that Rab7-WT and Rab7-Q67L were co-localized with the immature gp100 in Stage I melanosomes led us to investigate whether Rab7 activity plays a pivotal role in the regulation of the proteolytic cleavage of gp100. To quantify mature gp100, we carried out Western blot analysis of lysates from MMAc cells expressing Rab7-WT and its mutants using the anti-gp100 antibody HMB45, which recognizes only the cleaved, mature forms of gp100. It was confirmed that the mature gp100 was detected as several bands in the 30-kDa range including 32- and 29-kDa bands (Figure 4a, top panel), which are due to proteolytic cleavage at multiple sites during the maturation (Hoashi et al., 2006; Yasumoto et al., 2004). Interestingly, we found that overexpression of the dominant-active mutant (Rab7-Q67L) and, to a lesser extent, Rab7-WT significantly increased the protein levels of the processed, mature forms of gp100 (32- and 29-kDa bands) (Figure 4a, top panel and b). However, although the dominant-negative mutant (Rab7-T22N) was expressed to almost the same or rather higher extents compared with the WT protein and the dominant-active mutant, respectively (Figure 4a, lower middle panel), the mutant did not show such effect. Rab7-T22N, if any, slightly decreased the protein levels of the mature forms of gp100 (Figure 4b). On the other hand, the amounts of full-length gp100 (100-kDa band) were not markedly changed by the expression of Rab7-WT and Rab7-Q67L (Figure 4a, upper middle panel and c). These results suggest that Rab7 increased the amounts of mature gp100 by enhancing its post-translational modification (proteolytic cleavage) but not its transcription/translation.

As shown in Figure 4b, the dominant-negative mutant (Rab7-T22N) only slightly decreased the protein levels of the mature forms of gp100. We speculated that the relatively low effectiveness was probably caused by the low transfection efficiencies (around 40%) of Rab7 cDNA constructs to MMAc cells. It should be also noted that endogenous Rab7 is highly expressed (when detected by anti-Rab7 antibody, signal intensities of the over-expressed Rab7 bands were at most only two-fold higher than those of endogenous Rab7) (data not shown). Thus, to circumvent the problem of the low transfection efficiency, we performed siRNA experiments because the transfection efficiency of short RNA (siRNA) is much higher (> 80%) than that of long DNA (Rab7 cDNA constructs). Indeed, siRNA that specifically targets Rab7 (Jager et al., 2004) successfully and significantly reduced Rab7 protein expression (76.7 ± 6.3% decrease (mean ± S.E., n=4)) in MMAc cells (Figure 5a, top panel) as reported by Jager et al. (Jager et al., 2004). In marked contrast to the over-expression experiments (Figure 4a, top panel and b), the Rab7 siRNA significantly reduced the protein levels of mature gp100 (32- and 29-kDa bands) compared with the control siRNA (Figure 5a, upper middle panel and b). It is expected that the levels of the 100-kDa band should increase if the processing is disrupted. Indeed, the amount of full-length gp100 (100-kDa band) was slightly but clearly augmented by the Rab7 knockdown (Figure 5a, lower middle panel and c). It is also possible that the siRNA knockdown of Rab7 leads to mis-targeting rather than defects in processing (proteolysis). However, abnormal localization of gp100 was not observed in MMAc cells transfected with Rab7 siRNA (data not shown). Taken together, these results further support that Rab7 enhances the maturation of gp100 by promoting the proteolytic cleavage of gp100 in Stage I melanosomes.

DISCUSSION

Melanosome biogenesis consists of complex multi-step processes that involve protein synthesis, vesicle transport/fusion and post-translational modifications such as glycosylation, proteolysis and oligomerization. Moreover, these processes are regulated in a complicated manner. Because of the complexity, the detailed molecular mechanism of melanosome biogenesis is still elusive. Particularly, gp100 is one of the most enigmatic proteins involved in the melanogenesis. In the present study, we revealed that Rab7 may play an important role in promoting the gp100 maturation. Thus, Rab7 positively regulates the process of melanosome biogenesis via not only the transport of TYRP-1and tyrosinase (Gomez et al., 2001; Hirosaki et al., 2002) but also the maturation of gp100. Melanins are deposited on the fibrillar matrix formed by the mature gp100, resulting in a progressively pigmented internal matrix (Theos et al., 2005). Thus, a disruption of the gp100 maturation caused by the Rab7 dysfunction would lead to a delay and/or a reduction of the pigmentation. However, further studies are required to elucidate how the reduced amount of mature gp100 generally affects melanogenesis.

Rab7-Q67L and Rab7-WT were mainly localized in Stage I melanosomes where the full-length, immature gp100 was present (Figures 1 - 3), but not in Stage II and later Stage melanosomes containing the mature gp100. Therefore, these findings allow us to speculate that Rab7 is not involved in the later stages of gp100 maturation processes including stabilization and fibrous matrix formation. Hence, it is possible that Rab7 plays important roles in the expression of gp100 and/or early processes of its maturation such as transport to Stage I melanosomes and proteolysis there. Since the amount of full-length gp100 (precursor, 100-kDa band in Figure 4a) was not affected by the over-expression of Rab7-Q67L and Rab7-WT, it is likely that Rab7 participates in the early processes of gp100 maturation in the stage I melanosomes but not in the regulation of its expression. Although we analyzed the subcellular localization of gp100 in MMAc cells transfected with Rab7 siRNA, no significant changes were detected (data not shown). Thus, we consider that defects in processing, instead of mis-targeting, of gp100 are the most probable explanation for our results. If gp100 processing is accelerated (Figure 4), it is predicted that the levels of the full-length gp100 should be decreased. However, the amounts of the precursor, full-length gp100 were not changed (Figures 4). As shown in Figure 5c, the amount of the full-length gp100 was slightly augmented by the Rab7 knockdown. However, this slight increase does not fully explain the marked decease of the mature 29/32-kDa bands (Figure 5b). Although the precise mechanism is still unknown, a potential explanation of these results is that, in the maturation pathway, the cleavage step may be rate-limiting. In the experiment given in Figure 4, it is also expected that the amounts of the C-terminal-proteolytic product (27-kDa band in Figure 4a, upper middle panel), which is also recognized by □PEP13h, as well as the mature forms of gp100 (32- and 29-kDa bands in Figure 4a, top panel) are simultaneously increased because of the enhanced processing (proteolysis) of the full-length gp100 (see Figure 3a). Although significantly increased levels of the mature forms were detected, however, such an increase of the C-terminal 27-kDa band was not observed (data not shown). The most probable explanation of this result is that only the mature forms of gp100 are stably accumulated in melanosomes, whereas the C-terminal 27-kDa fragment is rapidly degraded (Yasumoto et al., 2004).

Two possible mechanisms are estimated to promote the gp100-processing: (1)

Rab7 enhances the transport of gp100 itself to Stage I melanosomes where gp100 is processed; (2) Rab7 promotes the transport of enzymes and their regulators that participate in the processing of gp100. As for the first possibility, gp100 is reported to be transported from the TGN to Stage I melanosomes directly and/or indirectly via the plasma membrane and early/late endosomes (Raposo et al., 2001; Valencia et al., 2006). Thus, it is possible that Rab7 associated with Stage I melanosomes promotes vesicle trafficking and membrane fusion between melanosomes and either the TGN or early/late endosomes. We previously reported that Rab7 is involved in the transport of TYRP-1 and tyrosinase from the TGN to melanosomes (Gomez et al., 2001; Hirosaki et al., 2002). Thus, it is interesting to speculate that there are common transport mechanisms underlying the conveyance of TYRP-1/tyrosinase and gp100 to their destination, melanosomes.

Next, regarding to the second possibility, several factors were reported to participate in the proteolysis of gp100. For instance, pro-hormone convertase, which exists in the endoplasmic reticulum, TGN, exocytotic vesicles, endosomes and melanosomes (Peters et al., 2000; Thomas, 2002), was reported to cleave gp100 (Berson et al., 2003). MART-1 interacts with gp100, and is involved in its expression, stabilization, transport and cleavage (Hoashi et al., 2005). Overexpression of myosin Ib caused a marked delay of the gp100 proteolysis (Salas-Cortes et al., 2005). Thus, Rab7 may positively (pro-hormone convertase and MART-1) or negatively (myosin Ib) regulate the supply (transport) of, at least, one of these factors to melanosomes, and thereby control the gp100 processing/maturation. Further work is required to elucidate which one of these factors/mechanisms is directly responsible for the Rab7-dependent gp100 maturation.

The maturation (glycosylation) of TYRP-1 and tyrosinase occurs in the Golgi apparatus. Thus, when restricted to "maturation", the effect of Rab7 is likely to be specific for gp100. However, melanosome biogenesis consists of multiple steps such as the transport of structural and enzymatic proteins and their subsequent structural organization as well as melanin deposition. Therefore, we rather consider that Rab7 comprehensively and cooperatively regulates melanosome biogenesis via controlling the transport of TYRP-1 and tyrosinase, and the maturation (proteolytic cleavage) of gp100.

In summary, this study, dealing with the complex multi-step processes of melanosome biogenesis, has provided several lines of evidence indicating that Rab7 is involved in gp100 maturation, enhancing its processing in Stage I melanosomes. Rab7 plays important roles in many vesicle transport pathways. Thus, future studies exploring how Rab7 regulates the gp100 maturation will provide further insights into not only the melanogenesis but also general mechanisms of vesicle transport regulated by Rab7.

MATERIALS AND METHODS

Plasmid constructs

pGEM-canine Rab7 was prepared as described previously (Bucci et al., 1994; Chavrier et al., 1990). Rab7-Q67L (a GTPase-deficient, dominant-active mutant), and Rab7-T22N (a GDP-bound, dominant-negative mutant) were generated using the QuikChange Site-directed Mutagenesis Kit (Stratagene, La Jolla, CA). These wild-type and mutant cDNAs of Rab7 were fused in frame with pEYFP-C1 (Takara-Clontech, Tokyo, Japan) and p3xFLAG-CMV-7.1 (Sigma-Aldrich, Tokyo, Japan).

Cell culture and transfection

MMAc human melanoma cells were kindly gifted from Dr. Tetsuya Moriuchi and Dr. Jun-ichi Hamada (Institute for Genetic Medicine, Hokkaido University School of Medicine, Sapporo, Japan). MMAc cells were maintained in Dulbeccos modified Eagle's medium (Sigma-Aldrich) containing 10% fetal bovine serum at 37 °C in an atmosphere of 5% CO_2. MMAc cells were transiently transfected with cDNAs using Effectene transfection reagent (Qiagen, Tokyo, Japan) according to the instructions from the manufacturer. Two days after transfection, cells were harvested for further analysis.

RNA interference

To silence the expression of human Rab7 (GenBank accession number: NM 004637), the following oligonucleotides (iGENE Therapeutics, Tsukuba, Japan), which had already been reported to successfully knockdown Rab7 (Jager et al., 2004), were used: 5'-cgguuccagucucucggug-ag-3' and its complementary sequence (5'-caccgagagacuggaaccg-au-3') (nucleotides 205–223 in the open reading frame). As a negative control, the following oligonucleotides targeting green fluorescent protein, which is not expressed in mammalian cells, were used: 5'-acggcaucaaggugaacuucaagau-ag-3' and its complementary sequence 5'-aucuugaaguucaccuugaugccgu-au-3'. The annealed oligonucleotide duplex was transfected into cells using HiPerFect Transfection Reagent (Qiagen) according to the instructions from the manufacturer. Three days after transfection, cells were harvested for further analysis.

Antibodies

Anti-Rab7 rabbit polyclonal antibody was raised against the C-terminal peptide of Rab7 (KQETEVELYNEFPEPIKLDKNDRAKTSAESCSC, amino acids 175-207) (Chavrier et al., 1990; Dong et al., 2004; Feng et al., 1995). □PEP13h (rabbit polyclonal antibody) reactive to the full-length gp100 and its truncated C-terminus was a kind gift from Dr. Vincent J. Hearing (Laboratory of Cell Biology, National Cancer Institute, National Institutes of Health, Bethesda, MD). HMB45 (mouse monoclonal antibody) for the processed internal domain of gp100 was purchased from Lab Vision (Fremont, CA). Anti-LAMP-2 mouse monoclonal and anti-actin goat polyclonal antibodies were purchased from Research Diagnostics (Concord, MA) and Santa Cruz Biotechnology (Santa Cruz, CA), respectively. Anti-FLAG M2 mouse monoclonal antibody was purchased from Sigma-Aldrich.

Western blot analysis

MMAc cells grown on 60-mm dishes were transiently trasnfected with siRNAs or plasmids encoding different forms of Rab7. Mock transfections were performed using empty vectors. Transfected MMAc cells were washed twice with phosphate-buffered saline (PBS). The transfected cells were lysed in 500 □l lysis buffer containing 150 mM NaCl, 20 mM Tris-HCl, pH 7.4, 1 mM EDTA, 1 mM phenylmethylsulfonyl fluoride, Protease inhibitor cocktail (one tablet/50 ml, Roche Diagnostics, Tokyo, Japan). After cells were lysed by sonication, followed by a centrifugation at 400 x g for 5 min, the supernatant was mixed with its one fourth volume of sodium dodecyl sulfate (SDS)-sample buffer (125 mM Tris-HCl, pH 6.8, 10% SDS, 50% glycerol, 10% 2-mercaptoethanol, 0.005% bromophenol blue), and

boiled for 5 min. Protein concentrations were measured using the BCA protein assay (Pierce Biotechnology, Rockford, IL). Equal amounts of protein were separated on 12% SDS-PAGE. The separated proteins were transferred to a polyvinylidene difluoride membrane (Bio-Rad Laboratories, Tokyo, Japan) and blocked with Block Ace (Dainippon Pharmaceutical, Tokyo, Japan). The membrane was incubated with either □PEP13h, HMB45, anti-actin antibody, anti-FLAG M2 antibody or anti-Rab7 antibody in 10% Block Ace for one hour. The immunoreactive bands were visualized using peroxidase-conjugated anti-mouse, anti-rabbit, or anti-goat IgG antibody (Jackson ImmunoResearch Laboratories, West Grove, PA) and the ECL Plus Western blotting detection system (GE Healthcare Bio-Sciences, Piscataway, NJ). To measure the relative density of immunoreactive bands, images were scanned and analyzed by Image J software (National Institute of Health, Bethesda, MD).

Fluorescence microscopy

MMAc cells were grown on poly-L-lysine-coated glass coverslips and transiently transfected with the control vector or cDNAs encoding Rab7-WT and its mutants fused with YFP. After 2 days, MMAc cells were washed twice with PBS and fixed with 3.7% formaldehyde in PBS for 10 min at room temperature. After washing twice with PBS, the cells were permeabilized with 0.1% Triton X-100 in PBS for 5 min at room temperature. After washing twice with PBS, the cells were incubated in PBS containing 2% BSA for 30 min at room temperature as a blocking step. The cells were then incubated in 10% Block Ace/PBS containing □PEP13h, HMB45 or anti-LAMP-2 for one hour at room temperature. This was followed by incubation with the corresponding secondary antibodies, i.e. goat anti-rabbit IgG or goat anti-mouse IgG coupled with Alexa Fluor 594 (Molecular Probes, Eugene, Oregon). The coverslips were mounted using Vectashield (Vector Laboratories, Burlingame, CA). Stains in cells were observed using an inverted confocal laser scanning microscope (Zeiss LSM 510). Images were processed using Adobe Photoshop 8.0.1 (Adobe Systems, San Jose, CA).

CONFLICT OF INTEREST

The authors state no conflict of interest.

ACKNOWLEDGMENTS

This work was supported in part by grants from the Ministry of Education, Culture, Sports, Science and Technology, the Japanese Government. We thank Drs. Tetsuya Moriuchi and Jun-ichi Hamada (Institute for Genetic Medicine, Hokkaido University, Sapporo, Japan) for providing MMAc human melanoma cells. We thank Dr. Vincent J. Hearing (National Cancer Institute, National Institutes of Health, Bethesda, MD) for the kind gift of anti-gp100 antibody (□PEP13h).

REFERENCES

Berson JF, Theos AC, Harper DC, Tenza D, Raposo G, Marks MS (2003) Proprotein convertase cleavage liberates a fibrillogenic fragment of a resident glycoprotein to initiate melanosome biogenesis. J Cell Biol **161**:521-533.

Bucci C, Thomsen P, Nicoziani P, McCarthy J, van Deurs B (2000) Rab7: a key to lysosome biogenesis. Mol Biol Cell **11**:467-480.

Bucci C, Wandinger-Ness A, Lutcke A, Chiariello M, Bruni CB, Zerial M (1994) Rab5a is a common component of the apical and basolateral endocytic

machinery in polarized epithelial cells. Proc Natl Acad Sci U S A **91**:5061-5065.

Cantalupo G, Alifano P, Roberti V, Bruni CB, Bucci C (2001) Rab-interacting lysosomal protein (RILP): the Rab7 effector required for transport to lysosomes. EMBO J **20**:683-693.

Chabrillat ML, Wilhelm C, Wasmeier C, Sviderskaya EV, Louvard D, Coudrier E (2005) Rab8 regulates the actin-based movement of melanosomes. Mol Biol Cell **16**:1640-1650.

Chavrier P, Parton RG, Hauri HP, Simons K, Zerial M (1990) Localization of low molecular weight GTP binding proteins to exocytic and endocytic compartments. Cell **62**:317-329.

De Maziere AM, Muehlethaler K, van Donselaar E, Salvi S, Davoust J, Cerottini JC, et al. (2002) The melanocytic protein Melan-A/MART-1 has a subcellular localization distinct from typical melanosomal proteins. Traffic **3**:678-693.

Dong J, Chen W, Welford A, Wandinger-Ness A (2004) The proteasome a-subunit XAPC7 interacts specifically with Rab7 and late endosomes. J Biol Chem **279**:21334-21342.

Feng Y, Press B, Wandinger-Ness A (1995) Rab 7: an important regulator of late endocytic membrane traffic. J Cell Biol **131**:1435-1452.

Gomez PF, Luo D, Hirosaki K, Shinoda K, Yamashita T, Suzuki J, et al. (2001) Identification of rab7 as a melanosome-associated protein involved in the intracellular transport of tyrosinase-related protein 1. J Invest Dermatol **117**:81-90.

Harrison RE, Bucci C, Vieira OV, Schroer TA, Grinstein S (2003) Phagosomes fuse with late endosomes and/or lysosomes by extension of membrane protrusions along microtubules: role of Rab7 and RILP. Mol Cell Biol **23**:6494-6506.

Hirosaki K, Yamashita T, Wada I, Jin HY, Jimbow K (2002) Tyrosinase and tyrosinase-related protein 1 require Rab7 for their intracellular transport. J Invest Dermatol **119**:475-480.

Hoashi T, Muller J, Vieira WD, Rouzaud F, Kikuchi K, Tamaki K, et al. (2006) The repeat domain of the melanosomal matrix protein PMEL17/GP100 is required for the formation of organellar fibers. J Biol Chem **281**:21198-21208.

Hoashi T, Watabe H, Muller J, Yamaguchi Y, Vieira WD, Hearing VJ (2005) MART-1 is required for the function of the melanosomal matrix protein PMEL17/GP100 and the maturation of melanosomes. J Biol Chem **280**:14006-14016.

Jager S, Bucci C, Tanida I, Ueno T, Kominami E, Saftig P, et al. (2004) Role for Rab7 in maturation of late autophagic vacuoles. J Cell Sci **117**:4837-4848.

Jimbow K, Park JS, Kato F, Hirosaki K, Toyofuku K, Hua C, et al. (2000) Assembly, target-signaling and intracellular transport of tyrosinase gene family proteins in the initial stage of melanosome biogenesis. Pigment Cell Res **13**:222-229.

Johansson M, Lehto M, Tanhuanpaa K, Cover TL, Olkkonen VM (2005) The oxysterol-binding protein homologue ORP1L interacts with Rab7 and alters functional properties of late endocytic compartments. Mol Biol Cell **16**:5480-5492.

Kuroda TS, Ariga H, Fukuda M (2003) The actin-binding domain of Slac2-a/melanophilin is required for melanosome distribution in melanocytes. Mol Cell Biol **23**:5245-5255.

Meresse S, Gorvel JP, Chavrier P (1995) The rab7 GTPase resides on a vesicular compartment connected to lysosomes. J Cell Sci **108**:3349-3358.

Mizuno K, Kitamura A, Sasaki T (2003) Rabring7, a novel Rab7 target protein with a RING finger motif. Mol Biol Cell **14**:3741-3752.

Peters EM, Tobin DJ, Seidah NG, Schallreuter KU (2000) Pro-opiomelanocortin-related peptides, prohormone convertases 1 and 2 and the regulatory peptide 7B2 are present in melanosomes of human melanocytes. J Invest Dermatol **114**:430-437.

Pfeffer SR (1999) Transport-vesicle targeting: tethers before SNAREs. Nat Cell Biol **1**:E17-22.

Press B, Feng Y, Hoflack B, Wandinger-Ness A (1998) Mutant Rab7 causes the accumulation of cathepsin D and cation-independent mannose 6-phosphate receptor in an early endocytic compartment. J Cell Biol **140**:1075-1089.

Raposo G, Tenza D, Murphy DM, Berson JF, Marks MS (2001) Distinct protein sorting and localization to premelanosomes, melanosomes, and lysosomes in pigmented melanocytic cells. J Cell Biol **152**:809-824.

Salas-Cortes L, Ye F, Tenza D, Wilhelm C, Theos A, Louvard D, et al. (2005) Myosin Ib modulates the morphology and the protein transport within multi-vesicular sorting endosomes. J Cell Sci **118**:4823-4832.

Somsel Rodman J, Wandinger-Ness A (2000) Rab GTPases coordinate endocytosis. J Cell Sci **113**:183-192.

Stein MP, Feng Y, Cooper KL, Welford AM, Wandinger-Ness A (2003) Human VPS34 and p150 are Rab7 interacting partners. Traffic **4**:754-771.

Strom M, Hume AN, Tarafder AK, Barkagianni E, Seabra MC (2002) A family of Rab27-binding proteins. Melanophilin links Rab27a and myosin Va function in melanosome transport. J Biol Chem **277**:25423-25430.

Takai Y, Sasaki T, Matozaki T (2001) Small GTP-binding proteins. Physiol Rev **81**:153-208.

Theos AC, Truschel ST, Raposo G, Marks MS (2005) The Silver locus product Pmel17/gp100/Silv/ME20: controversial in name and in function. Pigment Cell Res **18**:322-336.

Thomas G (2002) Furin at the cutting edge: from protein traffic to embryogenesis and disease. Nat Rev Mol Cell Biol **3**:753-766.

Valencia JC, Watabe H, Chi A, Rouzaud F, Chen KG, Vieira WD, et al. (2006) Sorting of Pmel17 to melanosomes through the plasma membrane by AP1 and AP2: evidence for the polarized nature of melanocytes. J Cell Sci **119**:1080-1091.

Vitelli R, Santillo M, Lattero D, Chiariello M, Bifulco M, Bruni CB, et al. (1997) Role of the small GTPase Rab7 in the late endocytic pathway. J Biol Chem **272**:4391-4397.

Wu X, Rao K, Bowers MB, Copeland NG, Jenkins NA, Hammer JA, 3rd (2001) Rab27a enables myosin Va-dependent melanosome capture by recruiting the myosin to the organelle. J Cell Sci **114**:1091-1100.

Yasumoto K, Watabe H, Valencia JC, Kushimoto T, Kobayashi T, Appella E, et al. (2004) Epitope mapping of the melanosomal matrix protein gp100 (PMEL17): rapid processing in the endoplasmic reticulum and glycosylation in the early Golgi compartment. J Biol Chem **279**:28330-28338.

Zerial M, McBride H (2001) Rab proteins as membrane organizers. Nat Rev Mol Cell Biol **2**:107-117.

FIGURE LEGENDS

Figure 1. Rab7-WT and Rab7-Q67L are co-localized with full-length, immature gp100 in the perinuclear region. MMAc cells were transfected with either the pEYFP empty vector, pEYFP-Rab7-WT, pEYFP-Rab7-Q67L, or pEYFP-Rab7-T22N (green). After 2 days, the cells were fixed and immunostained with □PEP13h and Alexa Fluor 594-conjugated secondary antibody (red). Bars, 10 □m. Insets, 2x magnification of the indicated regions. Structures co-localized for full-length gp100 and either Rab7-WT or Rab7-Q67L are indicated by arrowheads.

Figure 2. Rab7-WT and Rab7-Q67L are co-localized with LAMP-2 in the perinuclear region. MMAc cells were transfected with either the pEYFP empty vector, pEYFP-YFP-Rab7-WT, pEYFP-YFP-Rab7-Q67L, or pEYFP-YFP-Rab7-T22N (green). After 2 days, the cells were fixed and immunostained with anti-LAMP-2 antibody and Alexa Fluor 594-conjugated secondary antibody (red). Bars, 10 □m. Insets, 2x magnification of the indicated regions. Structures co-localized for LAMP-2 and either Rab7-WT or Rab7-Q67L are indicated by arrowheads.

Figure 3. Rab7-WT and Rab7-Q67L fails to be co-localized with processed, mature gp100. (a) Schematic presentation of the processing and epitope mapping of gp100 (Yasumoto et al., 2004). gp100 is shown as the complete native protein at the top of the Figure and in its processed/matured forms in the middle and at the bottom of the Figure. Potential N-glycosylation sites at 81, 106, 111, 321, and 568 are indicated. Val-467 (V467) refers to the potential cleavage site (CS) during maturation of Stage I to Stage II melanosomes. TM, transmembrane domain; inverted Ys, antibodies. (b) MMAc cells were transfected with either pEYFP-Rab7-WT or pEYFP-Rab7-Q67L (green). After 2 days, the cells were fixed and immunostained with HMB45 and Alexa Fluor 594-conjugated secondary antibody (red). Bars, 10 □m.

Figure 4. Overexpression of Rab7-WT and Rab7-Q67L promotes the maturation of gp100. (a) MMAc cells were transfected with either the p3xFLAG-CMV empty vector, p3xFLAG-CMV-Rab7-WT, p3xFLAG-CMV-Rab7-Q67L, or p3xFLAG-CMV-Rab7-T22N. After 2 days, the cells were harvested and analyzed by Western blotting using anti-FLAG M2 antibody, □PEP13h, HMB45, or anti-actin antibody as indicated. Equal amounts of protein were loaded in each lane. (b and c) The band intensities of mature gp100 (32- + 29-kDa bands detected by HMB45) (b) and full-length gp100 (100-kDa band detected by □PEP13h) (c) were quantified and then normalized for those of actin. The results represent the means ± SEM of the values obtained in five separate experiments. The value of p3xFLAG-CMV vector-transfected cells was set at 100.

Figure 5. Downregulation of Rab7 expression with siRNA inhibits the maturation of gp100. (a) MMAc cells were transfected with control siRNA or Rab7 siRNA. After 3 days, the cells were harvested and analyzed by Western blotting using anti-Rab7 antibody, □PEP13h, HMB45, or anti-actin antibody as indicated. Equal amounts of protein were loaded in each lane. (b and c) The band intensities of mature gp100 (32- + 29-kDa bands detected by HMB45) (b) and full-length gp100 (100-kDa band detected by □PEP13h) (c) were quantified and then normalized for those of actin. The results represent the means ± SEM of the values obtained in four separate

experiments. The value of control siRNA-transfected cells was set at 100.

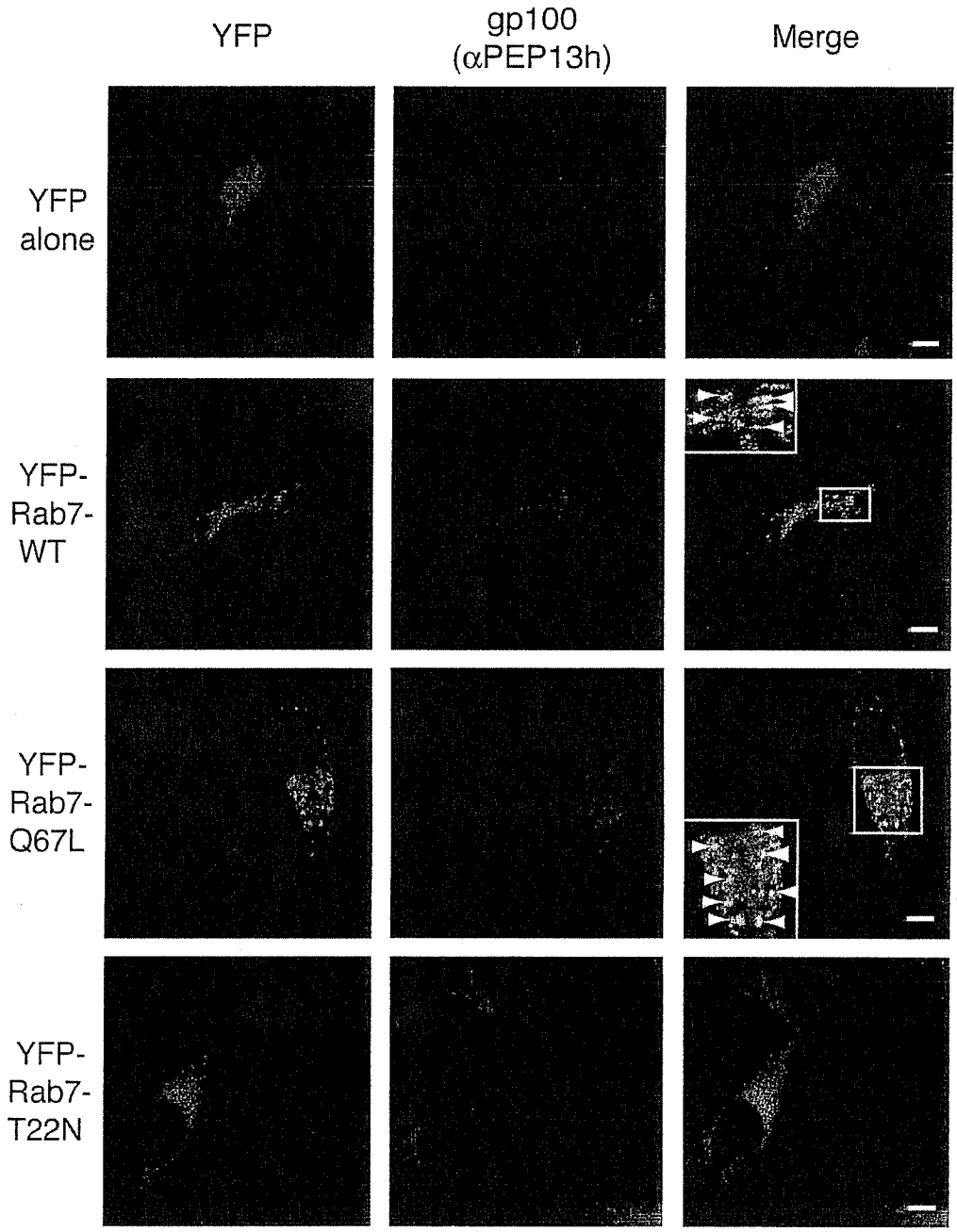

Fig. 1 KAWAKAMI et al.

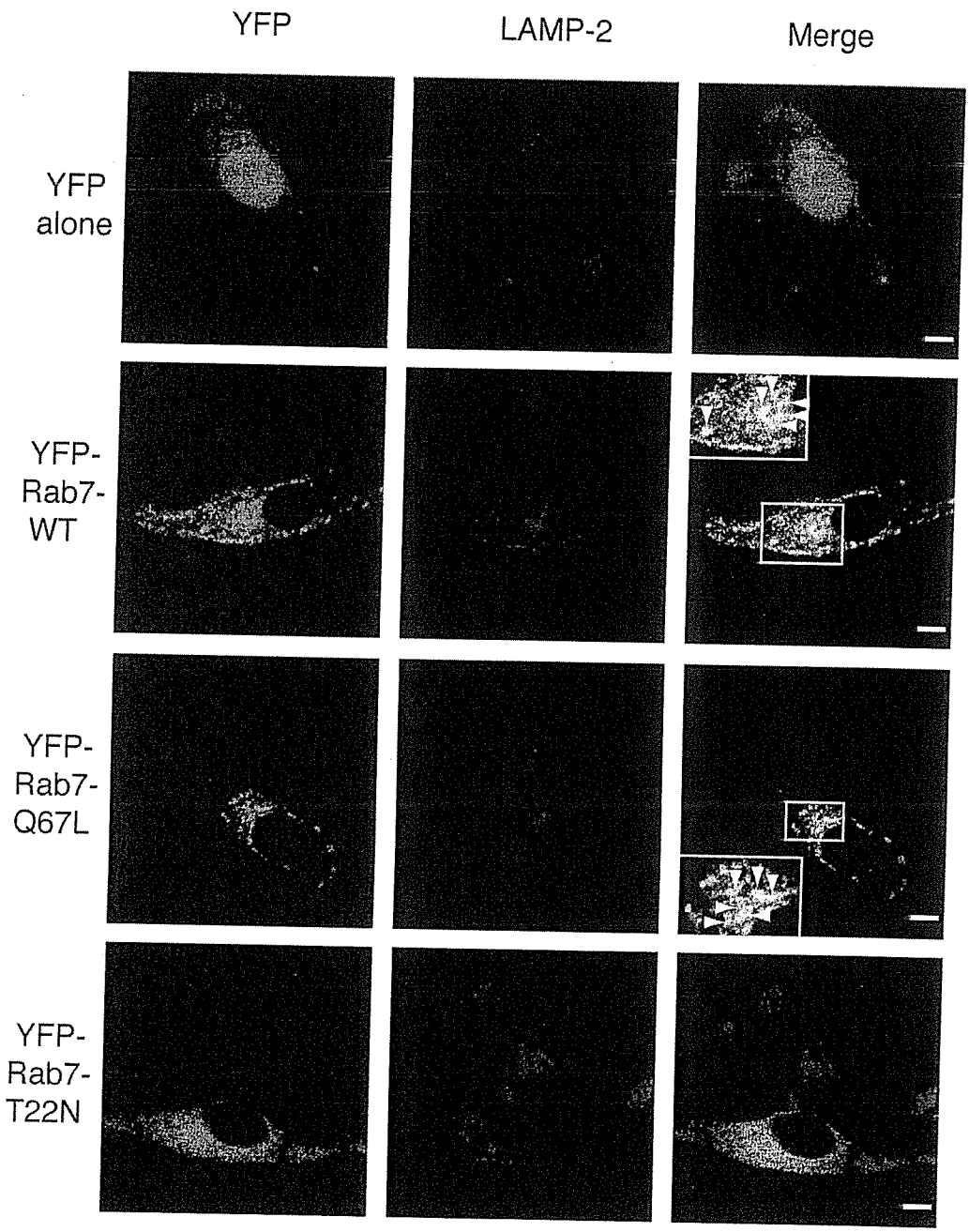

Fig. 2 KAWAKAMI et al.

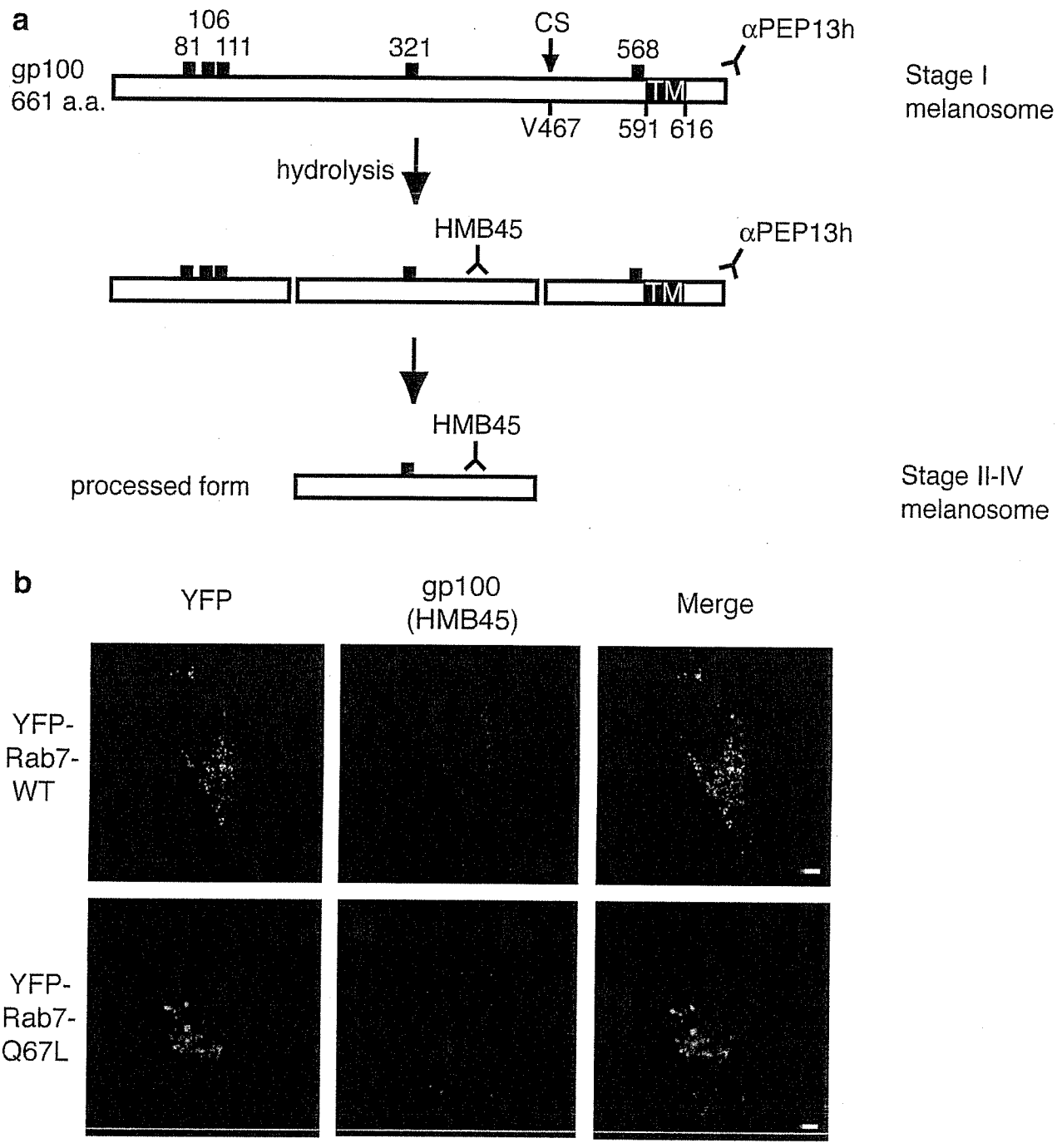

Fig. 3 KAWAKAMI et al.

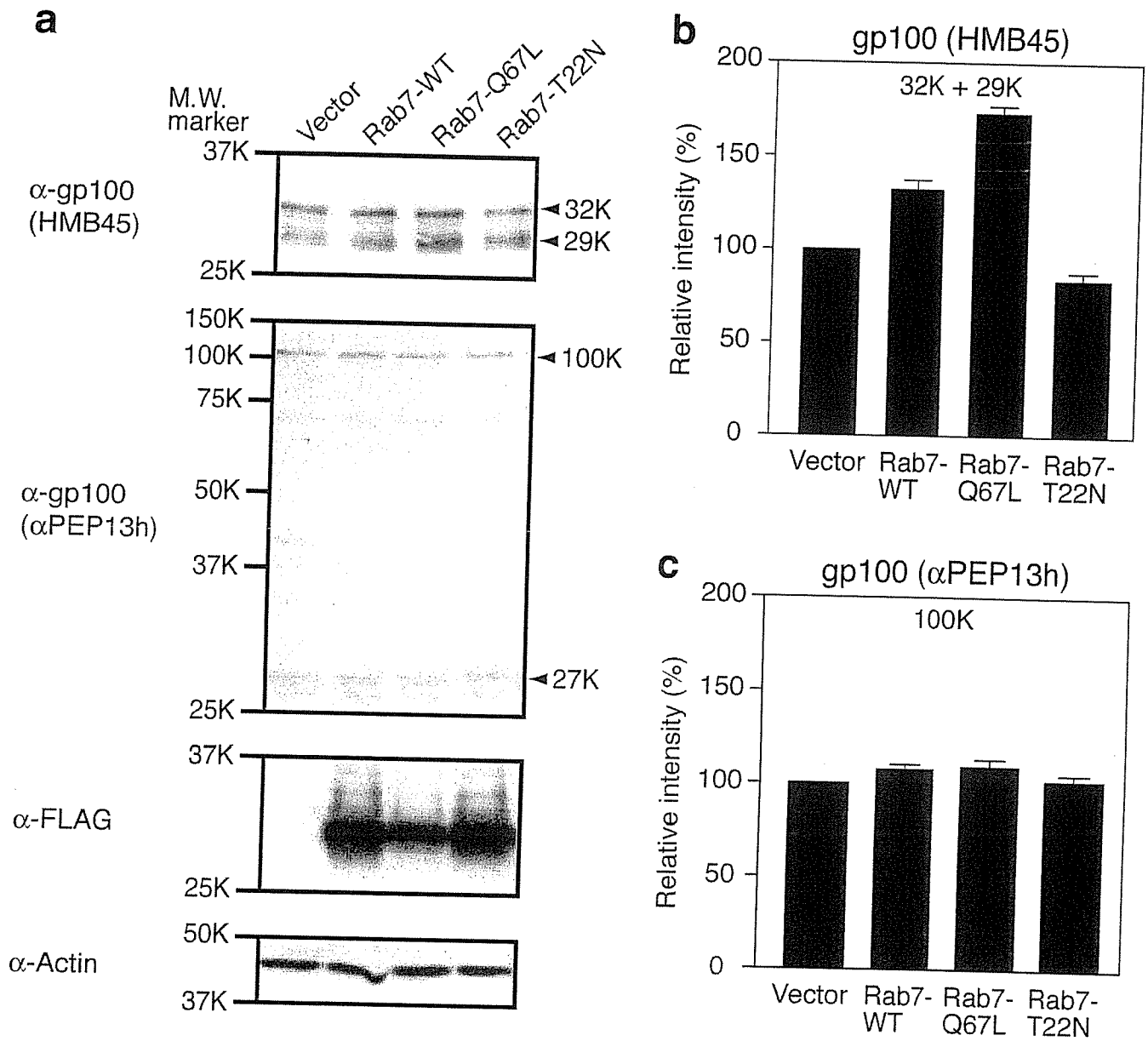

Fig. 4 KAWAKAMI et al.

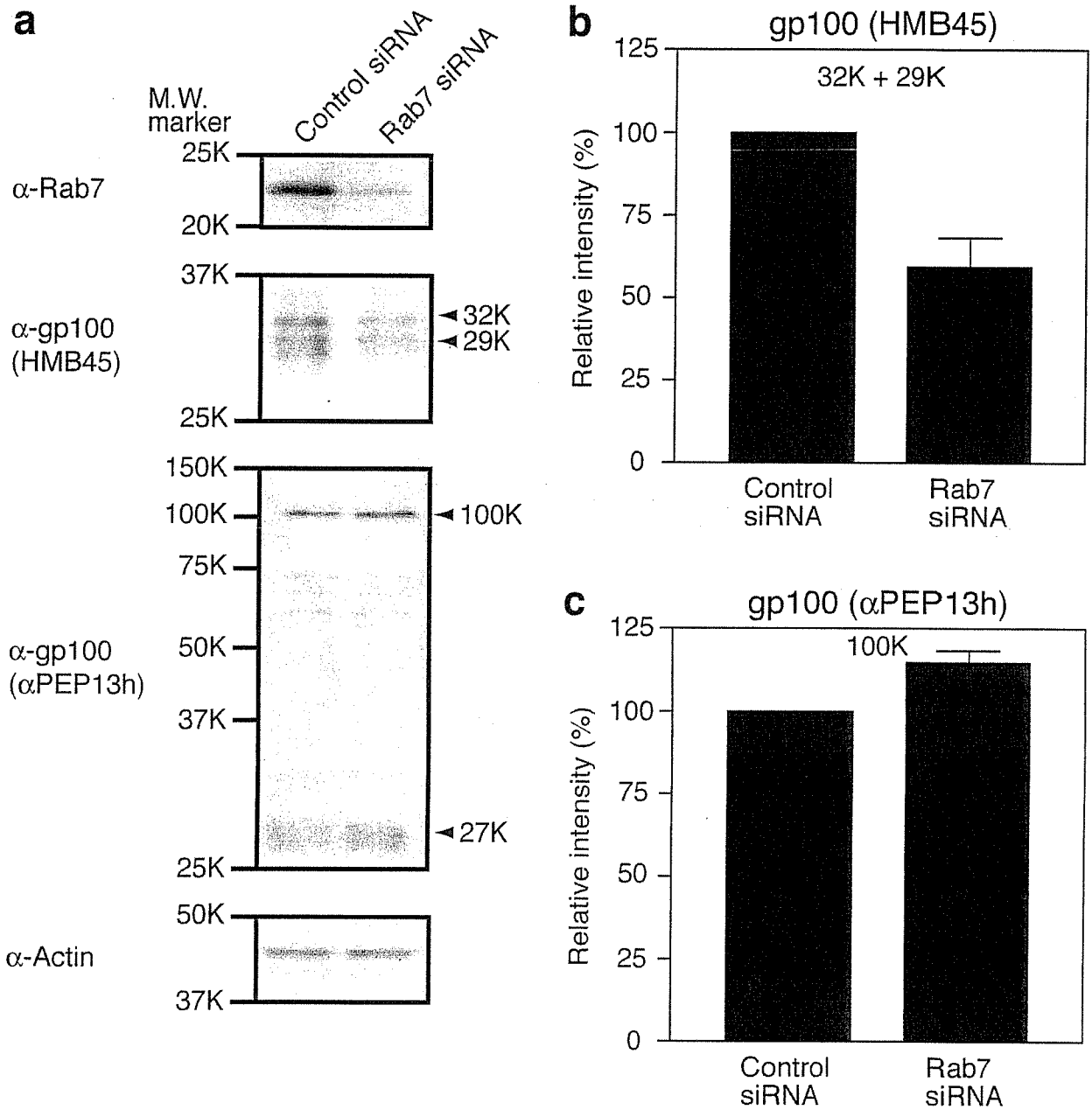

Fig. 5 KAWAKAMI et al.

4-*S*-Cysteaminylphenol-loaded magnetite cationic liposomes for combination therapy of hyperthermia with chemotherapy against malignant melanoma

Akira Ito,[1] Masatake Fujioka,[2] Tatsuro Yoshida,[2] Kazumasa Wakamatsu,[3] Shosuke Ito,[3] Toshiharu Yamashita,[4] Kowichi Jimbow[4] and Hiroyuki Honda[2,5]

[1]Department of Chemical Engineering, Faculty of Engineering, Kyushu University, 744 Mototoka, Nishi-ku, Fukuoka 819-0395; [2]Department of Biotechnology, School of Engineering, Nagoya University, Furo-cho, Chikusa-ku, Nagoya 464-8603; [3]Department of Chemistry, Fujita Health University School of Health Sciences, Toyoake, Aichi 470-1192; [4]Department of Dermatology, Sapporo Medical University School of Medicine, South 1 West 17, Chuo-ku, Sapporo 060-8556, Japan

(Received June 28, 2006/Revised October 26, 2006/Accepted October 31, 2006/Online publication December 22, 2006)

Tyrosine analogs are good candidates for developing melanoma chemotherapies because melanogenesis is inherently toxic and expressed uniquely in melanocytic cells. The sulfur homolog of tyrosine, 4-*S*-cysteaminylphenol (4-*S*-CAP), was shown to be a substrate of melanoma tyrosinase and can cause selective cytotoxicity of melanocytes and melanoma cells. Previously, in order to improve the adsorption of magnetite nanoparticles to target cell surfaces, and generate heat in an alternating magnetic field (AMF) for cancer hyperthermia, we produced hyperthermia using magnetite cationic liposomes (MCL) that have a positive charge at the liposomal surface. In the present study, we constructed 4-*S*-CAP-loaded MCL (4-*S*-CAP/MCL), which act as a novel modality, combining melanoma-specific chemotherapy by 4-*S*-CAP with intracellular hyperthermia mediated by MCL. The 4-*S*-CAP/MCL exerted 4-*S*-CAP-mediated anticancer effects on B16 melanoma cells *in vitro* and *in vivo*. Moreover, after intratumoral injection of 4-*S*-CAP/MCL *in vivo*, the melanoma nodules were heated to 45°C under an AMF. Significantly higher therapeutic effects were observed in mice treated with the combination therapy mediated by 4-*S*-CAP/MCL plus AMF irradiation compared with mice treated with 4-*S*-CAP/MCL alone (without AMF) or mice treated with hyperthermia alone (MCL + AMF irradiation). These results suggest that this novel therapeutic tool is applicable to the treatment of malignant melanoma. (*Cancer Sci* 2007; 98: 424–430)

Hyperthermia is a promising approach to cancer therapy and has been used for many years to treat a wide variety of tumors in both experimental animals and patients.[1] In Japan, the most commonly used heating method in clinical settings is capacitive heating using a radiofrequency electric field.[2] An unavoidable technical problem with hyperthermia is the difficulty in heating only the local tumor region to the intended temperature without damaging the surrounding healthy tissue. Specifically, heating tumors by capacitive heating using a radiofrequency electric field is difficult because various factors, such as tumor size, position of electrodes, and adhesion of electrodes at uneven sites, influence the heating characteristics. Hyperthermia produced by heating mediators is a promising approach for specifically heating tumors without damaging normal tissues.[3] Magnetite nanoparticles have been used for hyperthermia treatment in an attempt to overcome this obstacle.[4–6] If magnetite nanoparticles can be made to accumulate only in tumor tissue, cancer-specific hyperthermia can be achieved by generating heat in an alternating magnetic field (AMF) due to hysteresis loss. In order to test this hypothesis, we developed magnetite cationic liposomes (MCL) as mediators of intracellular hyperthermia.[7–9] These cationic liposomes exhibit improved adsorption and accumulation in tumor cells, and have 10-fold higher affinity for tumor cells than neutrally charged magnetoliposomes,[7] thus suggesting that MCL are superior mediators of hyperthermia. We previously demonstrated the efficacy of MCL-mediated hyperthermia in animals with several cell lines, including T-9 rat glioma,[9] Os515 hamster osteosarcoma,[10] MM46 mouse mammary carcinoma,[11] PLS 10 rat prostate cancer,[12] and VX-7 squamous cell carcinoma in rabbit tongue.[13] Although MCL-mediated hyperthermia was found to be very effective for inducing complete tumor regression in transplantable tumor models, more powerful therapies are highly desired for cancer patients with malignancy.

Among the various forms of neoplasmas of the skin, malignant melanoma is the most invasive tumor. Various medical therapies, such as surgery, chemotherapy, radiotherapy and immunotherapy, are commonly used in the treatment of melanoma patients; however, none of these has proved sufficiently effective. Therefore, an effective protocol for the prevention and treatment of melanoma is needed urgently. Given this background, the combination of chemotherapy with MCL-mediated hyperthermia can be considered a possible strategy, because both magnetite nanoparticles and anticancer drugs can be encapsulated simultaneously into a liposome.

Tyrosine analogs are good candidates for developing melanoma chemotherapy because melanogenesis is inherently toxic and uniquely expressed in melanocytic cells. We introduced the use of phenolic thioether analogs of tyrosine for targeted melanoma chemotherapy based on the idea that the incorporation of sulfur would render the phenolics more cytotoxic by increased lipophilicity leading to increased uptake by cells, thus making them better substrates for tyrosinase.[14] Therefore, we synthesized the sulfur homolog of tyrosine, 4-*S*-cysteaminylphenol (4-*S*-CAP), in order to develop a targeted chemotherapy for malignant melanoma.[14,15] 4-*S*-CAP was found to be a substrate of melanoma tyrosinase and can cause selective cytotoxicity of melanocytes and melanoma cells.[16] In the present study, we constructed 4-*S*-CAP-loaded magnetite cationic liposomes (4-*S*-CAP/MCL) and investigated the feasibility of using them for combined melanoma-targeted chemotherapy and tumor-specific hyperthermia.

Materials and Methods

Cell lines and animal models. Mouse B16 melanoma cells were cultured in Dulbecco's modified Eagle's medium (Gibco BRL, Gaithersburg, MD, USA), supplemented with 10% fetal calf serum, 0.1 mg/mL streptomycin sulfate and 100 IU/mL potassium penicillin G. Normal human dermal fibroblasts (NHDF) were provided as frozen cells after primary culture by the supplier (Kurabo, Osaka, Japan), and were cultured in commercially available growth media (Medium106S; Kurabo) at 37°C in a humidified atmosphere of CO_2 and 95% air.

[5]To whom correspondence should be addressed. E-mail: honda@nubio.nagoya-u.ac.jp

doi: 10.1111/j.1349-7006.2006.00382.x

To prepare tumor-bearing mice, 8×10^5 B16 melanoma cells were injected subcutaneously into the right flank of C57BL/6 mice, which were anesthetized by intraperitoneal injection of pentobarbital (50 mg/kg bodyweight). Melanoma nodules that had grown to 5 mm in diameter were used for experiments. Tumor diameter was measured using calipers and the average size was determined by applying the following formula:

$$\text{Tumor size} = 0.5 \times (\text{length} + \text{width}),$$

where length and width were measured in mm.

Animal experiments were carried out according to the principles described in the 'Guide for the Care and Use of Laboratory Animals' prepared under the direction of the Prime Minister of Japan.

Analysis of the combined effect of 4-*S*-CAP and hyperthermic treatment. B16 cells were plated in six-well cell culture plates at 4×10^4 cells/well with experimental media containing 4-*S*-CAP at a concentration of 50 μM. The cells were then treated with hyperthermic treatment using a water bath. Hyperthermic treatment of cultured cells was carried out as in our previous report.[17] Briefly, the cells were heated to 42.5°C for 60 min by direct immersion of cell culture dishes in a temperature-controlled water bath. The temperature of the medium increased quickly and reached the intended temperature within 5 min. The temperature of the medium was monitored using a fiber optic thermometer probe (FX-9020; Anritsu Meter, Tokyo, Japan). Control cells were not treated with 4-*S*-CAP or hyperthermia.

The antiproliferative effect of the treatment was determined after a 2-day incubation period. The number of viable cells was evaluated by the trypan blue dye-exclusion method using a hemocytometer, and the relative cell number was calculated as follows:

$$\text{Relative cell number (\%)} = (\text{number of viable experimental cells/number of viable control cells}) \times 100.$$

The combined effect of 4-*S*-CAP and hyperthermia was evaluated using a method reported previously.[18] With [A], [B] and [A + B] representing the percentage cell viability for treatments A and B and the combination treatment A + B, the combined effects were defined as follows: synergistic, $[A + B] < [A] \times [B]/100$; additive, $[A + B] = [A] \times [B]/100$; subadditive, $[A] \times [B]/100 < [A + B] < [A]$, if $[A] < [B]$; interference, $[A] < [A + B] < [B]$, if $[A] < [B]$; and antagonistic, $[B] < [A + B]$, if $[A] < [B]$.

Preparation of 4-*S*-CAP/MCL. Magnetite nanoparticles (Fe_3O_4; average particle size, 10 nm) were the kind gift of Toda Kogyo (Hiroshima, Japan). 4-*S*-CAP was synthesized as described by Padgette *et al.*[19] For the preparation of 4-*S*-CAP/MCL, 0–32 mg of 4-*S*-CAP was added to a lipid mixture consisting of *N*-(α-trimethylammonioacetyl)-didodecyl-D-glutamate chloride (2.78 mg; Sogo Pharmaceutical, Tokyo, Japan), dilauroylphosphatidylcholine (6.64 mg; Sigma Chemical, St Louis, MO, USA) and dioleoylphosphatidyl-ethanolamine (5.58 mg; Sigma Chemical) dissolved in methanol (2 mL), and the mixture was dried down by evaporation for a minimum of 5 h. Then, the lipids containing 4-*S*-CAP were hydrated by vortexing with colloidal magnetite nanoparticles (20 mg/mL, 2 mL) and the liposomes were sonicated for 20 min (28 W). The size of the 4-*S*-CAP/MCL was measured using a dynamic light scattering spectrophotometer (FRAR 1000; Otsuka Electronics, Osaka, Japan).

Antiproliferative activity of 4-*S*-CAP in 4-*S*-CAP/MCL. B16 cells, or NHDF cells as a non-melanocytic control, were plated in six-well cell culture plates at 5×10^4 cells/well with experimental media containing 4-*S*-CAP/MCL at the indicated concentration. The antiproliferative activity was determined after the 2-day incubation period. The number of viable cells was measured by the trypan blue dye-exclusion method using a hemocytometer, and the relative cell number was calculated.

Uptake of 4-*S*-CAP/MCL by B16 cells. B16 cells were cultured to approximately 80% confluence before treatment with 4-*S*-CAP/MCL. Cells were then incubated with experimental media containing 4-*S*-CAP/MCL at a concentration of 43 μg magnetite/mL (4-*S*-CAP, 100 μM), and cells were incubated at 37°C with gentle shaking using a rotary shaker (SHK-320; Asahi Technoglass, Tokyo, Japan). After incubation for 24 h, the cells were washed twice with phosphate-buffered saline and harvested and the magnetite concentration was measured in accordance with our reported method.[7] Briefly, the harvested cells were dissolved completely in 0.2 mL of concentration HCl, after which 1 mL of 5% trichloroacetic acid was added. These mixtures were centrifuged in order to remove aggregates and the supernatants were measured by the potassium thiocyanate method.[20]

***In vitro* magnetite nanoparticle-induced hyperthermia.** An *in vitro* hyperthermia experiment using magnetite nanoparticles was carried out using our previously described method.[7] Briefly, B16 cells were cultured to approximately 80% confluence. Cells were then incubated with experimental media containing 4-*S*-CAP/MCL at a concentration of 43 μg magnetite/mL (4-*S*-CAP, 100 μM). At 24 h after the magnetite incorporation, the cells were collected in a microcentrifuge tube and centrifuged gently in order to form a cell pellet. The tube was then placed at the center of the coil of a high-frequency magnetic field generator (360 kHz, 120 Oe; Daiichi High Frequency, Tokyo, Japan). The temperature of the cell pellet was measured by inserting an optical fiber probe into its center, and the pellet was maintained at a constant temperature by manually tuning the strength of the magnetic field. The duration of the AMF irradiation was 30 min. During AMF irradiation, the temperature of the environment was maintained at 37°C. The treated cells were reseeded in a six-well cell culture plate at 2×10^4 cells/well. The number of viable cells was measured by the trypan blue exclusion method using a hemocytometer.

***In vivo* magnetite nanoparticle-induced hyperthermia.** When melanoma nodules grew to 5 mm in diameter, the tumor-bearing mice were separated into five groups (day 0). Mice in group I (control) were the non-treated control. Mice in groups II (MCL) and IV (MCL + AMF) received intratumoral injection of MCL (0.2 mL, 20 mg magnetite/mL). Mice in groups III (4-*S*-CAP/MCL) and V (4-*S*-CAP/MCL + AMF) received intratumoral injection of 4-*S*-CAP/MCL (0.2 mL; 20 mg/mL magnetite; 100 μM 4-*S*-CAP). At 1 day after the injection of MCL or 4-*S*-CAP/MCL (day 1), mice in groups IV (MCL + AMF) and V (4-*S*-CAP/MCL + AMF) were subjected to AMF for 30 min in a coil with a transistor inverter. Magnetic field frequency and intensity were 118 kHz and 384 Oe, respectively. Tumor and rectal temperatures were measured using an optical fiber probe. Subsequently, after the AMF irradiation, MCL or 4-*S*-CAP/MCL were again injected into the mice in groups II and IV or groups III and V, respectively. At 1 day after the second injection (day 2), mice in groups IV (MCL + AMF) and V (4-*S*-CAP/MCL + AMF) were again subjected to AMF for 30 min. During the injection of MCL or 4-*S*-CAP/MCL and AMF irradiation, tumor-bearing mice were anesthetized with pentobarbital sodium (50 mg/kg intraperitoneally).

For histological examination, the tumor was resected and fixed in a 10% formalin solution 24 h after hyperthermia. The specimens were fixed in 10% neutrally buffered formalin, and embedded in paraffin. Serial specimens were then prepared for histological examination, and were stained with hematoxylin and eosin (H&E).

Statistical analysis. Statistical analysis was carried out by the Mann–Whitney rank sum test calculated using WinSTAT statistical software (Light Stone International, Tokyo, Japan). Differences were considered to be statistically significant at $P < 0.05$.

Results

Combined effect of 4-*S*-CAP and hyperthermic treatment. Figure 1 shows the relative cell number for B16 cells on the second day

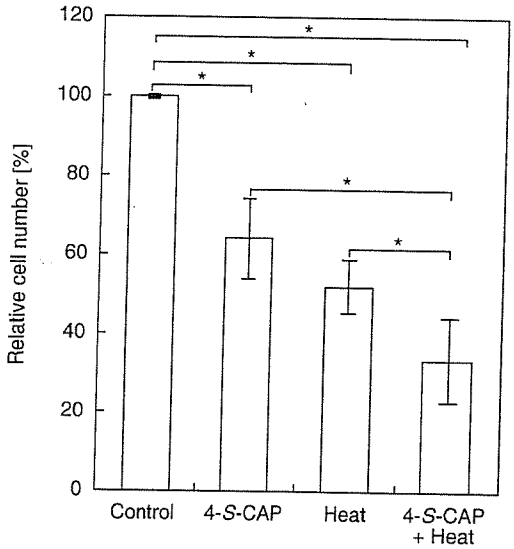

Fig. 1. Combined effects of 4-*S*-cysteaminylphenol (4-*S*-CAP) and heat treatment on B16 cell viability. B16 cells were treated with 4-*S*-CAP at 50 μM. Simultaneously, the cells were heated using a water bath at 42.5°C for 1 h. After the 2-day incubation period, antiproliferative effects were assessed as the relative cell number (%). Data and bars are mean ± SD of two independent experiments. $*P < 0.05$.

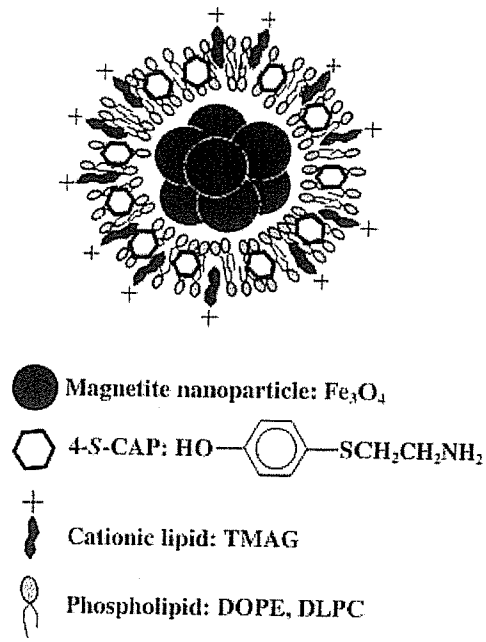

Fig. 2. Preparation of 4-*S*-cysteaminylphenol (4-*S*-CAP)/magnetite cationic liposomes (MCL). Illustration of 4-*S*-CAP/MCL is shown.

after hyperthermic treatment using a 42.5°C water bath for 60 min. For hyperthermic treatment alone, the relative cell number was 52.5 ± 6.6%. For 4-*S*-CAP (50 μM) treatment alone, the relative cell number was 64.4 ± 9.9%. When hyperthermic treatment was combined with 4-*S*-CAP treatment, the relative cell number decreased to 33.7 ± 10.6%. With [A], [B] and [A + B] representing the percentage cell viability for treatments of 4-*S*-CAP, heat and the combination treatment 4-*S*-CAP + heat, respectively, the combined effects were defined as follows: synergistic, [A + B] < [A] × [B]/100; additive, [A + B] = [A] × [B]/100; subadditive, [A] × [B]/100 < [A + B] < [A], if [A] < [B]; interference, [A] < [A + B] < [B], if [A] < [B]; and antagonistic, [B] < [A + B], if [A] < [B]. Here, [A + B] and [A] × [B]/100 were 33.7 ± 10.6% and 34.1 ± 9.5%, respectively. Because there was no significant difference ($P = 0.56$) between [A + B] and [A] × [B]/100, the combined effect of 4-*S*-CAP with heat was evaluated as additive effects.

Preparation of 4-*S*-CAP-loaded MCL. Because the combination of 4-*S*-CAP and hyperthermia has an additive effect, we constructed 4-*S*-CAP/MCL (Fig. 2) and investigated whether 4-*S*-CAP/MCL can combine 4-*S*-CAP-mediated chemotherapy with MCL-induced hyperthermia. The size distribution of 4-*S*-CAP/MCL with various 4-*S*-CAP contents was measured using a dynamic light-scattering spectrophotometer (Fig. 3). For MCL without 4-*S*-CAP, the peak in the particle size distribution was 124.5 ± 0.95 nm (the mean ± SD of three independent experiments). The average size of 4-*S*-CAP/MCL increased drastically when the 4-*S*-CAP concentration exceeded 100 μM. When the 4-*S*-CAP concentration exceeded 100 μM, the dispersibility of 4-*S*-CAP/MCL was extremely low and precipitation of 4-*S*-CAP/MCL was observed. Therefore, 4-*S*-CAP/MCL at 100 μM of 4-*S*-CAP concentration was used in the following *in vivo* experiments.

Antiproliferative activity of 4-*S*-CAP in 4-*S*-CAP/MCL. Figure 4a shows the antiproliferative effects of different concentrations of 4-*S*-CAP/MCL on B16 cells. The dose–response curve showed a dose-dependent antiproliferative effect for 4-*S*-CAP in 4-*S*-CAP/MCL, with the maximum effects achieved using a concentration of 400 μM (46.6 ± 0.9% of relative cell number), which was comparable to the cytotoxicity of free 4-*S*-CAP (inhibition

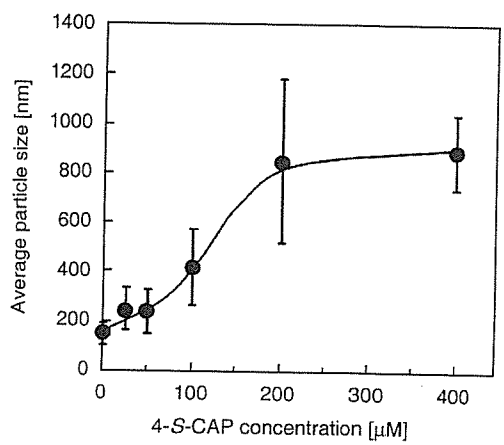

Fig. 3. Relationship between 4-*S*-cysteaminylphenol (4-*S*-CAP) concentration and liposome size of 4-*S*-CAP/magnetite cationic liposomes (MCL). The size of the 4-*S*-CAP/MCL was measured using a dynamic light scattering spectrophotometer. Data and bars are mean ± SD of three independent experiments.

concentration [IC_{50}] IC_{50} of 507 μM) toward B16 melanoma cells.[21] Figure 4b shows the time course of the relative cell number when B16 or NHDF cells were treated with 100 μM 4-*S*-CAP/MCL. The relative cell number for B16 cells decreased linearly to 60% during the 2-day culture period. In contrast, non-melanocytic NHDF cells showed no decrease in relative cell number 1 day after 4-*S*-CAP/MCL treatment, with only slight antiproliferative effects (15% decrease in the relative cell number) observed on day 2. These results indicate that 4-*S*-CAP in 4-*S*-CAP/MCL had an antiproliferative effect on B16 cells, although 4-*S*-CAP was less toxic to non-melanocytic NHDF cells, an observation that corresponds to previous reports.[22]

Uptake of magnetite nanoparticles by B16 cells and *in vitro* hyperthermia. Next, in order to assess the feasibility of magnetite nanoparticle-mediated hyperthermia *in vitro*, we investigated whether 4-*S*-CAP/MCL

doi: 10.1111/j.1349-7006.2006.00382.x